ARCHIVE OF MECHANICAL ENGINEERING

DOI: 10.24425/ame.2025.157602 2026, Vol. 73, No. 1, pp. 103–123

Vineet Kumar VERMA [1], JANHVI [1]

Magnetohydrodynamic boundary layer flow of copper and silver nanofluids over a permeable moving plate in a porous medium

Received 21 December 2024, **Revised** 22 November 2025, **Accepted** 27 November 2025, **Published online** 27 December 2025

Keywords: magnetic field, porous medium, thermal radiation, viscous dissipation, permeable moving flat plate

This study investigates the flow and heat transfer characteristics of copper (Cu) and silver (Ag) nanofluids over a permeable, moving flat plate embedded in a porous medium under the influence of a uniform magnetic field. Key effects such as thermal radiation, viscous dissipation, nanoparticle volume fraction, and suction/injection are incorporated into the model. The governing partial differential equations are reduced to ordinary differential equations using similarity transformations and solved numerically via the Runge-Kutta fourth-order method with a shooting technique. Results reveal that Ag-water nanofluid exhibits a higher temperature profile, whereas Cu-water shows greater skin friction and heat transfer rates. Velocity decreases with increasing magnetic field strength, porosity, volume fraction, and suction/injection parameters. Thermal boundary layer thickness increases with magnetic and porosity parameters but decreases with stronger suction. The Nusselt number increases with nanoparticle concentration, and temperature rises with higher viscous dissipation but decreases with thermal radiation.

Nomenclature

B_0	External magnetic field	k^*	Absorption coefficient
Br	Brinkmann number	k_{nf}	Thermal conductivity of the nanofluid
C_f	Skin friction coefficient	M	Magnetic parameter
c_p	Specific heat at constant pressure	Nu	Local Nusselt number
K	Permeability of porous medium	Pr	Prandtl number

✉ Janhvi, email: janhvi1612@gmail.com

[1]Department of Mathematics and Astronomy, University of Lucknow, Lucknow, India

R	Radiation parameter	T_w	Plate surface temperature
r_v	Velocity ratio parameter	T_∞	Free stream temperature
Re_x	Reynolds number	U_w	Plate uniform velocity
S_w	Suction/injection parameter	U_∞	Free stream velocity
T	Temperature		

Greek symbols

α_{nf}	Thermal diffusivity of the nanofluid	ρ_f	Density of the base fluid
η	Dimensionless similarity variable	ρ_{nf}	Density of the nanofluid
θ	Dimensionless temperature	ρ_s	Density of the nanoparticles
λ	Porosity parameter	σ	Electrical conductivity of the fluid
μ_f	Dynamic viscosity of the base fluid	τ_w	Surface shear stress
μ_{nf}	Dynamic viscosity of the nanofluid	ϕ	Solid volume fraction
ν_f	Kinematic viscosity of the base fluid	ψ	Stream function

Subscripts

∞	Ambient condition	s	Solid phase
f	Base fluid	w	Wall/surface condition
nf	Nanofluid		

Abbreviations

MHD	Magnetohydrodynamics
ODEs	Ordinary Differential Equations
PDEs	Partial Differential Equations

1. Introduction

The nanofluid is the concoction of nano-sized (1–100 nm) particles called nanoparticles, made of copper, carbon, aluminum, silver, iron, etc. They are suspended in conventional heat transfer fluids such as water, oil, ethylene glycol, etc. In recent times, nanofluids are used in numerous industrial engineering applications such as wire drawing, pharmaceutical processes, domestic refrigerators, glass-fiber production, fuel cells, microelectronics, etc. Nanofluids can also be used as coolants for cooling of nuclear reactors, compact heat exchangers, fusion control, casting, filtration of liquid metals, etc. The term "nanofluid" was first suggested by Choi and Eastman [1]. Nanoparticles can be produced from many materials by physical and chemical synthesis processes such as the mechanical grinding method, the inert-gas condensation technique, chemical precipitation, chemical vapor deposition, micro-emulsions, spray pyrolysis, thermal spraying, etc. Buongiorno [2] conducted a thorough analysis of convective transport in nanofluids. He provided a convincing justification for the unusual rise in viscosity and thermal conductivity in comparison to the base fluid.

Recently, the study of magnetohydrodynamic (MHD) boundary layer flow over moving surfaces as well as on stretching surfaces has drawn the attention of many researchers because of its critical role in numerous industrial and engineering

applications. Furthermore, magnetic nanofluids are significantly more prevalent in a wide range of industrial and scientific domains. Hydrodynamic assets, thermal energy transfer, and magnetic fields are all stimulated by these nanofluids. The impact of MHD nanofluid flow across an elongating flat plate was discussed by Sheikholeslami et al. [3] and Hatami et al. [4]. MHD mixed convection stagnation point flow of a hybrid nanofluid past a vertical flat plate with convective boundary condition was analyzed by Zainal et al. [5]. Furthermore, Khashi'ie et al. [6] investigated magnetohydrodynamics boundary layer flow of hybrid nanofluid over a moving plate with Joule heating.

Direct energy emission from the radiated surface in the form of an electromagnetic wave in all directions is known as thermal radiation. The thermal radiation effect is crucial to the flow of various liquids and heat transmission from an engineering and physical perspective. In engineering processes that need a high operating temperature, thermal radiation has been proven to be helpful. Among these are the designs of nuclear power plants, gas turbines, airplanes, spacecraft, dependable machinery, satellites, etc. [7]. The Rosseland approximation ([8, 9]), which treats thermal radiation as a diffusion mechanism, simplifies the intricate radiative transfer process and is used in this study to model it. This method simplifies the radiative heat flux equation for numerical analysis and works for optically thick mediums. Engineering procedures that call for high operating temperatures have been proven to benefit from thermal radiation. Recently, Jha and Samaila [7] analyzed the thermal radiation effect on boundary layer flow over a flat plate having convective surface boundary condition. The impact of thermal radiation on water-based hybrid nanofluid (Cu-Al_2O_3-H_2O) flow over a forward/backward moving vertical porous plate was observed by Arulmozhi et al. [10]. The effects of magnetic field and thermal radiation on the mixed convection of Al_2O_3-Cu/water hybrid nanofluid over a permeable vertical flat plate were studied by Jafaripournimchahi et al. [11].

The term "viscous dissipation" describes how internal friction in a fluid can transform mechanical energy into thermal energy. Numerous studies on fluid flow and heat transmission have been conducted to examine the impact of viscous thermal dissipation. These investigations showed that when studying convective heat transfer, fluid flows with a higher Eckert number produce heat due to viscous thermal dissipation and regulate the temperature. Additionally, the Eckert number cannot be zero [12]. The effect of viscous dissipation on heat transfer in capillary flow was examined by Brinkman [13]. Oyelami and Falodan [12] investigated the heat and mass transfer of hydrodynamic boundary layer flow along a flat plate with the influence of variable temperature and viscous dissipation. Khashi'ie et al. [14] studied the Blasius flow over a permeable moving flat plate containing Cu-Al_2O_3 hybrid nanoparticles with viscous dissipation and radiative heat transfer. The consequences of heat generation/absorption and suction/injection on MHD flow of Ag-water nanofluid past a stretching flat plate in a porous medium with Ohmic-viscous dissipation were analyzed by Upreti et al. [15]. Gopal et al. [16] scrutinized the numerical analysis of higher-order chemical reactions on electrically

MHD nanofluid under the influence of viscous dissipation. Kho et al. [17] studied the analysis of the magnetohydrodynamics flow of Ag-TiO_2 hybrid nanofluid over a permeable wedge with heat radiation and viscous dissipation.

For a flat plate, the standard component of the velocity at the wall must be equal to a predetermined value, which may be positive or negative, in order for suction injection to occur. The injection or suction parameter influences the fluid's temperature and velocity profiles in addition to the heat transfer and skin friction coefficients. The plate's aerodynamic performance may be enhanced by the suction or injection, which can also stop or postpone boundary layer separation. For many engineering applications, including the extrusion of metals and plastics, the chilling and drying of paper and textiles, and the regulation of hybrid laminar flow on wings, the effect of suction on flat plates is crucial [18]. Iranian et al. cite18 examine the Maxwell fluid flow on a flat plate in the presence of radiation, suction/injection, heat generation, slip circumstances, and velocity slip conditions. Hybrid nanofluid flow over a vertical flat plate with Marangoni convection in the presence of quadratic thermal radiation and an exponential heat source was investigated by Yaseen et al. [19]. Shuaib et al. [20] analyzed the problem of unsteady viscous nanofluid flow between two porous plates under the effect of a variable magnetic field and suction/injection.

Fluid flow through porous media, found in systems like soils, rocks, and filters, is crucial for fields like hydrology, petroleum engineering, and environmental science. Numerous studies are being conducted in these fields; recent ones, like [21–25], examined the impact of MHD on conducting fluid flow in rotating porous media with isotropic and anisotropic permeabilities. They also conducted an analytical investigation of the flow in an anisotropic porous channel with a single plate moving at a constant velocity [26]. The steady mixed convection boundary layer flow past a vertical flat plate embedded in a porous medium filled with nanofluids is studied by Ahmad and Pop [27] using different types of nanoparticles. Awasthi et al. [28] conducted a linear stability investigation of the capillary instability at the viscoelastic liquid-viscous gas interface, including heat and mass transmission. The issue of the anisotropy angle influence on Poiseuille flow and generalized Couette flow of micropolar fluids was investigated analytically by Verma and Ansari [29, 30].

The present model essentially extends the work of Motsumi and Makinde [31] to include the MHD boundary layer flow and porous medium. The aspiration of this present analysis is to investigate the mutual effects of the magnetic parameter, porosity parameter, radiation parameter, Brinkmann number, and suction/injection parameter on the MHD boundary layer flow of water-based nanofluids containing copper (Cu) and silver (Ag) nanoparticles in a porous medium. The governing partial differential equations are reduced into ordinary differential equations by using similarity transformation. The resulting problems are solved numerically using the Runge-Kutta fourth-order method with shooting technique. Appropriate results are presented graphically and discussed quantitatively.

2. Problem definition and solution

Consider a steady, laminar, incompressible two-dimensional magnetohydrodynamics (MHD) boundary layer flow of water-based nanofluids having nanoparticles (Cu and Ag) over a permeable flat plate situated in a porous medium with permeability K. The permeable flat plate is moving with a constant velocity U_w in the same or opposite direction of the free stream velocity U_∞. The x-axis is taken parallel to the plate surface, and the y-axis is taken perpendicular to the plate surface. A uniform magnetic field of strength B_0 is applied along the y-axis (Fig. 1). It is presumed here that the base fluid (water) and the nanoparticles are in thermal equilibrium and no slip occurs between them. The MHD boundary layer flow of nanofluids in the present analysis is governed by the following equations ([2, 32–36])

$$\frac{\partial u}{\partial x} + \frac{\partial u}{\partial y} = 0, \tag{1}$$

$$\rho_{nf}\left(u\frac{\partial u}{\partial x} + v\frac{\partial u}{\partial y}\right) = \mu_{nf}\frac{\partial^2 u}{\partial y^2} - \frac{\mu_{nf}}{K}u - \sigma B_0^2 u, \tag{2}$$

$$u\frac{\partial T}{\partial x} + v\frac{\partial T}{\partial y} = \alpha_{nf}\frac{\partial^2 T}{\partial y^2} + \frac{\mu_{nf}}{(\rho c_p)_{nf}}\left(\frac{\partial u}{\partial y}\right)^2 - \frac{1}{(\rho c_p)_{nf}}\left(\frac{\partial q_r}{\partial y}\right), \tag{3}$$

where u and v are the velocity components of the nanofluid in the x and y directions, respectively, and U_∞ is the constant free stream velocity. The continuity, momentum, and energy equations are represented by equations (1) through (3), respectively. The goal of the model is to represent how the temperature and flow velocity of nanofluids are affected by magnetic fields, porous media, thermal radiation, and viscous dissipation.

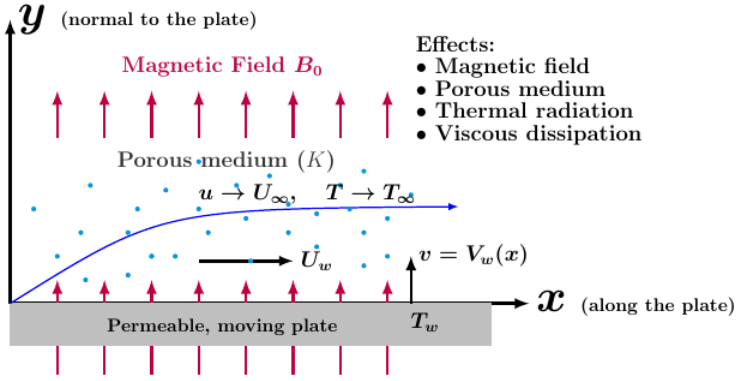

Fig. 1. Flow model of the problem

Thermophysical characteristics include, for example, the effective dynamic viscosity μ_{nf}, the effective density ρ_{nf}, the nanofluid's thermal diffusivity α_{nf}, the kinematic viscosity of the base fluid ν_f, the thermal conductivity k_{nf}, and the heat capacitance $(\rho c_p)_{nf}$, which are given by ([35, 36]).

$$\begin{aligned}
\mu_{nf} &= \frac{\mu_f}{(1-\phi)^{2.5}}\ , \\
\rho_{nf} &= (1-\phi)\rho_f + \phi\rho_s\ , \\
\alpha_{nf} &= \frac{k_{nf}}{(\rho c_p)_{nf}},\quad \nu_f = \frac{\mu_f}{\rho_f}, \\
k_{nf} &= k_f \frac{(k_s+2k_f) - 2\phi(k_s+2k_f)}{(k_s+2k_f) + \phi(k_s+2k_f)}, \\
(\rho c_p)_{nf} &= (1-\phi)(\rho c_p)_f + \phi(\rho c_p)_s.
\end{aligned} \tag{4}$$

According to the Rosseland approximation ([8] and [9]) for the thermal radiation, the radiative heat flux q_r is expressed as follows:

$$q_r = -\frac{4\sigma^*}{3k^*}\frac{\partial T^4}{\partial y}, \tag{5}$$

where σ^* is the Stephan-Boltzmann constant and k^* is the mass absorption coefficient. The temperature differences within the flow are assumed to be sufficiently small so that T^4 may be expressed as a linear function of temperature T using a truncated Taylor series about the free stream temperature T_∞, i.e.,

$$T^4 \approx 4T_\infty^3 T - 3T_\infty^4. \tag{6}$$

Using equations (5) and (6), equation (3) becomes

$$u\frac{\partial T}{\partial x} + v\frac{\partial T}{\partial y} = \left[\alpha_{nf} + \frac{1}{(\rho c_p)_{nf}}\frac{16\sigma^* T_\infty^3}{3k^*}\right]\frac{\partial^2 T}{\partial^2 y} + \frac{\mu_{nf}}{(\rho c_p)_{nf}}\left(\frac{\partial u}{\partial y}\right)^2. \tag{7}$$

The variable plate surface permeability function is given as

$$V_w = -\frac{S_w}{2}\sqrt{\frac{U\nu_f}{x}}, \tag{8}$$

where $U = U_w + U_\infty$, S_w is a constant with $S_w > 0$ representing the transpiration (suction) rate at the plate surface, $S_w < 0$ correlates to injection, and $S_w = 0$ for an impermeable surface. The velocity and temperature coupled boundary conditions at the plate surface and far into the nanofluid are written as ([35, 37])

$$\begin{aligned}
u(x,0) &= U_w, \qquad v(x,0) = V_w(x), \qquad T(x,0) = T_w, \\
u(x,\infty) &= U_\infty, \qquad T(x,\infty) = T_\infty
\end{aligned} \tag{9}$$

The stream function ψ satisfies the continuity equation (1) automatically with

$$u = \frac{\partial \psi}{\partial y} \qquad \text{and} \qquad v = -\frac{\partial \psi}{\partial x}. \tag{10}$$

Non-dimensional Variables

$$\begin{aligned} \eta &= y\sqrt{\frac{U}{\nu_f x}} = \frac{y}{x}\sqrt{\mathrm{Re}_x}, \\ \psi &= \sqrt{\nu_f U}\, f(\eta), \qquad u = U f'(\eta), \\ v &= \frac{1}{2}\sqrt{\frac{U\nu_f}{x}}(\eta f' - f), \\ \theta &= \frac{T - T_\infty}{T_w - T_\infty}, \end{aligned} \tag{11}$$

Our reduced governing equations are obtained by introducing the aforementioned dimensionless variables into governing equations (2) and (7) along with the boundary conditions in equation (9).

Reduced governing equations

$$f''' - \lambda(1-\phi)^{2.5}\left(1 - \phi + \phi\frac{\rho_s}{\rho_f}\right) f' - (1-\phi)^{2.5} M f' + \frac{1}{2}(1-\phi)^{2.5}\left(1 - \phi + \phi\frac{\rho_s}{\rho_f}\right) f f'' = 0, \tag{12}$$

$$\left(1 + \frac{4k_f}{3Rk_{nf}}\right)\theta'' + \frac{k_f Pr\left(1 - \phi + \phi\frac{(\rho c_p)_s}{(\rho c_p)_f}\right)}{2k_{nf}} f\theta' + \frac{k_f Br}{k_{nf}(1-\phi)^{2.5}}(f'')^2 = 0. \tag{13}$$

Boundary conditions

$$\begin{aligned} f(0) &= S_w, & f'(0) &= 1 - r_v, & \theta(0) &= 1, \\ f'(\infty) &= r_v, & \theta(\infty) &= 0. \end{aligned} \tag{14}$$

where the prime symbol denotes differentiation with respect to η.

In the governing equations, the parameters that are introduced are defined as the radiation parameter R, the porosity parameter λ, the magnetic parameter M, the Prandtl number Pr, the Brinkmann number Br, the local Reynolds number Re_x, and the velocity ratio parameter r_v are defined as follows:

$$R = \frac{k^* k_f}{4\sigma T_\infty^3}, \qquad \lambda = \frac{\nu_{nf} x}{KU}, \qquad M = \frac{\sigma B_0^2 x}{U\rho_f}, \qquad \mathrm{Pr} = \frac{\nu_f}{\alpha_f},$$
$$\mathrm{Br} = \frac{\mu_f}{U_\infty}, \qquad \mathrm{Re}_x = \frac{Ux}{\nu_f}, \qquad r_v = \frac{U_\infty}{U}.$$

The nanofluid motion is faster than the plate motion when $1 > r_v > 0.5$, while the plate motion is faster than the nanofluid motion when $0 < r_v < 0.5$. Both nanofluids and the plate are moving in the opposite direction when $r_v > 1$.

Local skin-friction coefficient C_f and local Nusselt number Nu are given by [31]

$$C_f = \frac{\tau_w}{\rho_f U_\infty^2}, \qquad \mathrm{Nu} = \frac{x q_w}{k_f (T_w - T_\infty)}, \tag{15}$$

where τ_w is the skin friction and q_w is the heat flux from the plate, given by

$$\tau_w = \left(\mu_{nf} \frac{\partial u}{\partial y}\Big|_{y=0}\right), \qquad q_w = -\left(k_{nf} + \frac{16\sigma T_\infty^3}{3k^*}\right)\frac{\partial T}{\partial y}. \tag{16}$$

Substituting equation (16) into equation (15), we get

$$\mathrm{Re}_x^{1/2} C_f = \left(\frac{1}{(1-\phi)^{2.5}}\right) f''(0), \qquad \mathrm{Re}_x^{-1/2}\mathrm{Nu} = -\left(\frac{k_{nf}}{k_f} + \frac{4}{3R}\right)\theta'(0). \tag{17}$$

The above set of equations (12) and (13), subject to the boundary conditions (14), were solved numerically by the Runge-Kutta fourth-order method with the shooting technique.Velocity and temperature profiles were obtained and utilized to calculate the skin friction coefficient C_f and the local Nusselt number Nu in equation (17). The thermophysical properties of water and nanoparticles of Cu and Ag are given in Table 1

Table 1. Thermophysical properties of Cu, Ag and water ([15, 31])

Physical properties	Fluid phase(water)	Cu	Ag
c_p	4179	385	235
ρ	997.1	8933	10500
k	0.613	400	429

3. Result and discussion

In this section, velocity and temperature profiles have been traced for two water-based nanofluids containing copper (Cu) and silver (Ag) nanoparticles. The analysis focuses on the influence of various parameters on the behavior of these profiles, as well as on the skin friction and local Nusselt number along the plate surface for both nanofluids. For the base fluid (water), a Prandtl number of 6.2 has been considered, consistent with its thermophysical properties under standard conditions.

3.1. Effects of different parameters on velocity profiles

Figures are plotted to analyze the impact of magnetic parameter M, porosity parameter λ, suction/injection parameter S_w, and the volume fraction parameter ϕ on velocity profiles and temperature profiles. From Figs. 2–5, the influence of different parameters on velocity profiles is shown.

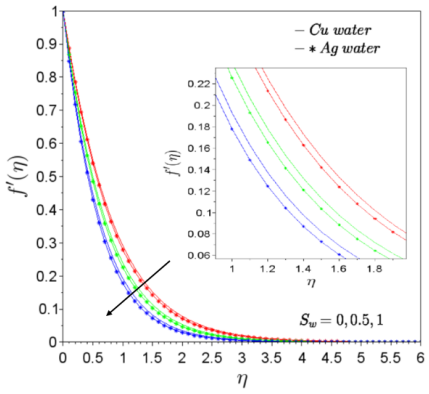

Fig. 2. Influence of suction parameter S_w on velocity profiles of Cu and Ag water nanofluids

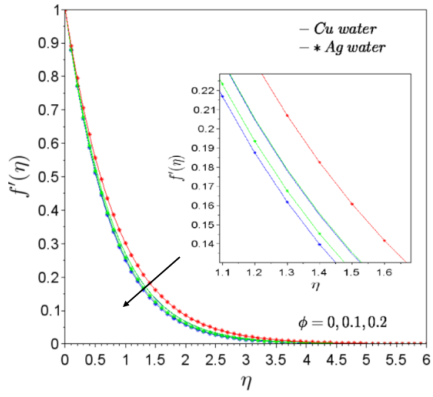

Fig. 3. Influence of volume fraction parameter ϕ on velocity profiles of Cu and Ag water nanofluids

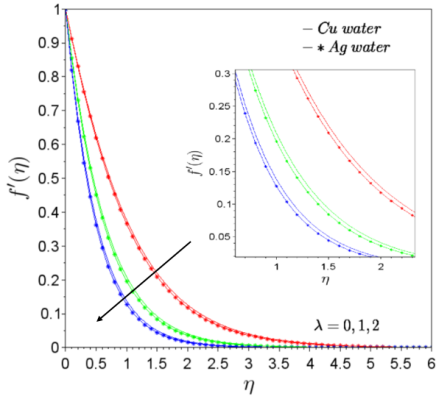

Fig. 4. Influence of porosity parameter λ on velocity profiles of Cu and Ag water nanofluids

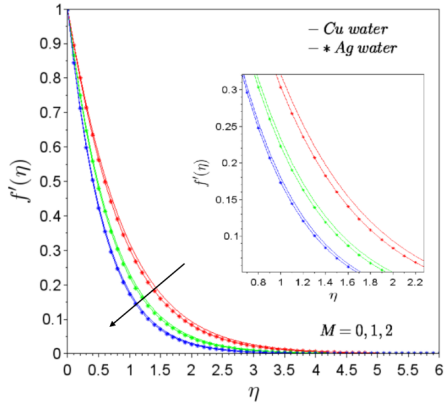

Fig. 5. Influence of magnetic number M on velocity profiles of Cu and Ag water nanofluids

Fig. 22 shows the effect of S_w on fluid velocity under various fixed parameters such as Pr = 6.2, M = 0.5, Br = 0.1, λ = 0.5, ϕ = 0.1, R = 1, and r_v = 0. Here, we conclude that on increasing the suction parameter (S_w), the velocity decreases because applying the suction parameter can effectively remove the fluid particles

near the plate surface, resulting in thinning of the boundary layer thickness, which means less fluid mass is moving at higher velocity near the boundary layer and causes an overall decrement in the velocity of fluid flow.

Fig. 3 represents the influence of ϕ on fluid velocity for some fixed parameters such as Pr = 6.2, $M = 0.5$, Br = 0.1, $S_w = 0.2$, $\lambda = 0.5$, $R = 1$, and $r_v = 0$. Here, velocity decreases with increasing solid volume fraction parameter ϕ. This is because of the fact that increasing the solid volume fraction of nanoparticles in the base fluid increases the fluid viscosity of the fluid, which makes the fluid more viscous, and also enhances the density of the fluid, due to which the fluid experiences greater resistance in its motion, and hence the boundary layer thickness decreases.

Fig. 4 shows the impact of λ on nanofluid velocity while other parameters are kept fixed, such as Pr = 6.2, $M = 0.5$, Br = 0.1, $S_w = 0.2$, $\phi = 0.1$, $R = 1$, and $r_v = 0$. Here we have shown that fluid velocity diminishes with the increasing porosity parameter λ. As we know, that fluid flow in a porous medium is described by Darcy's Law, which states that flow rate is proportional to pressure gradient and inversely proportional to the medium's permeability, K. Here, an increment in the porosity parameter does not increase the permeability proportionally and causes the overall reduction in the velocity profile.

Fig. 5 represents the effect of M on nanofluid velocity under various fixed parameters such as Pr = 6.2, $\lambda = 0.5$, Br = 0.1, $S_w = 0.2$, $\phi = 0.1$, $R = 1$, and $r_v = 0$. Here we observed that on increasing the magnetic number M, velocity decreases. The primary reason for the reduction in fluid velocity is that fluid particles experience Lorentz force, which creates more drag force on the fluid motion. Thus, it is concluded that the presence of this transverse magnetic force in the porous matrix leads to the retarding effect on velocity distribution, which decreases the momentum boundary layer thickness.

3.2. Effects of different parameters on temperature profiles

From Figs. 6–11, the impact of different parameters on temperature profiles is traced graphically.

Fig. 6 shows the effect of S_w on fluid temperature under various fixed parameters such as Pr = 6.2, $M = 0.5$, Br = 0.1, $\lambda = 0.5$, $\phi = 0.1$, $R = 1$, and $r_v = 0$. Suction removes fluid particles having high temperature near the plate surface and allows the fluid particles having low temperature, and this promotes the overall heat removal from the boundary layer, and as a result, the temperature of the fluid flow decreases and makes the thermal boundary layer thinner.

Fig. 7 represents the influence of ϕ on fluid temperature for some fixed parameters such as Pr = 6.2, $M = 0.5$, Br = 0.1, $S_w = 0.2$, $\lambda = 0.5$, $R = 1$, and $r_v = 0$. Here we observed that on increasing the solid volume fraction ϕ, temperature increases. Adding more nanoparticles to the fluid increases its thermal conductivity,

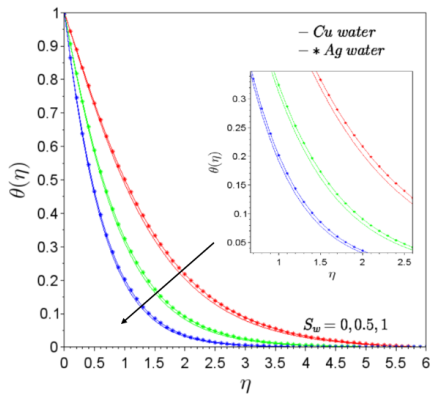

Fig. 6. Influence of suction parameter S_w on temperature profiles of Cu and Ag water nanofluids

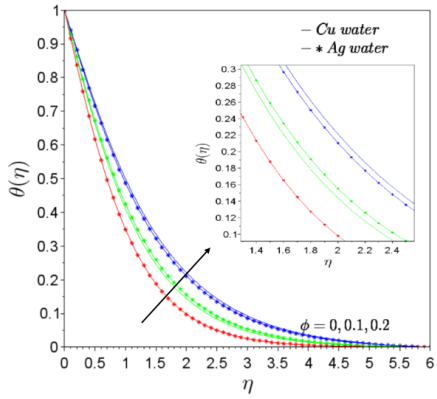

Fig. 7. Influence of volume fraction parameter ϕ on temperature profiles of Cu and Ag water nanofluids

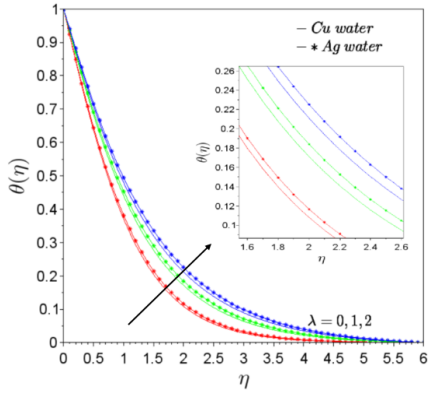

Fig. 8. Influence of porosity parameter λ on temperature profiles of Cu and Ag water nanofluids

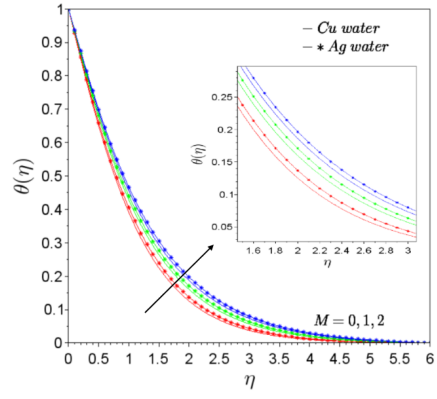

Fig. 9. Influence of magnetic number M on temperature profiles of Cu and Ag water nanofluids

and also, due to enhanced fluid viscosity, more internal resistance to flow means the temperature is higher, and hence, the thermal boundary layer thickness increases.

Fig. 8 shows the impact of λ on nanofluid temperature while other parameters are kept fixed, such as Pr = 6.2, M = 0.5, Br = 0.1, S_w = 0.2, ϕ = 0.1, R = 1, and r_v = 0. Here we find that on increasing the porosity parameter, temperature increases because more void spaces in the porous matrix are available for the air to trap sufficient heat to store more heat within the medium, which reduces the thermal conductivity of the nanofluid and causes the reduction in heat dissipation. Due to this reason, the thermal boundary layer width accelerates.

Fig. 9 represents the effect of M on nanofluid temperature under various fixed parameters such as Pr = 6.2, $\lambda = 0.5$, Br = 0.1, $S_w = 0.2$, $\phi = 0.1$, $R = 1$, and $r_v = 0$. Here, the graph shows that temperature increases on enhancing the strength of the magnetic field. As we have discussed earlier, on increasing Lorentz force, the velocity of the fluid flow decreases, and also because of the presence of a magnetic field, fluid viscosity increases, causing greater frictional heating within the fluid layers and retarding the velocity of the fluid flow, making the fluid's motion slower, thereby increasing the temperature of the nanofluids.

Fig. 10 represents the effect of Br on nanofluid temperature under various fixed parameters such as Pr = 6.2, $\lambda = 0.5$, $M = 0.5$, $S_w = 0.2$, $\phi = 0.1$, $R = 1$, and $r_v = 0$. Here, we observe that on increasing the values of the Brinkmann number Br, temperature increases due to viscous heating because an increase in the Brinkmann number generally results in a higher temperature due to the reduced efficiency of heat conduction compared to the heat generated by viscous forces.

Fig. 11 shows the impact of R on nanofluid temperature while other parameters are kept fixed, such as Pr = 6.2, $\lambda = 0.5$, $M = 0.5$, Br = 0.1, $S_w = 0.2$, $\phi = 0.1$, and $r_v = 0$. Here, we observed that on increasing the values of the radiation parameter R, temperature increases because an increased radiation parameter means that more heat is being transferred through radiation. This efficient heat transfer mechanism can help dissipate heat more effectively, leading to a decrease in temperature.

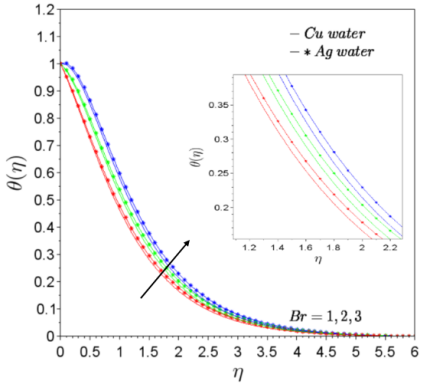

Fig. 10. Influence of Brinkmann parameter Br on temperature profiles of Cu and Ag water nanofluids

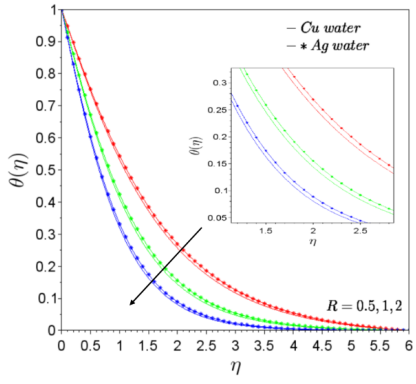

Fig. 11. Influence of radiation parameter R on temperature profiles of Cu and Ag water nanofluids

Fig. 12 shows the velocity profiles of Cu and Ag water nanofluids for the case when fluid flow over a stationary object is steered by the free stream velocity U_∞ (r_v=1) while some parameters are kept fixed, such as Pr = 6.2, λ, = 0.5, $M = 0.5$, Br = 0.1, $S_w = 0.2$, $\phi = 0.1$, $R = 1$, and $r_v = 1$. So, velocity gradually approaches the constant value 1, satisfying the far-field boundary condition. It is interesting to

note that the momentum boundary layer thickness for Ag-water is slightly lower than Cu-water.

Fig. 13 represents the temperature profiles of Cu and Ag water nanofluids under various fixed parameters such as Pr = 6.2, $\lambda = 0.5$, $M = 0.5$, Br = 0.1, $S_w = 0.2$, $\phi = 0.1$, $R = 1$, and $r_v = 1$. We have observed that Ag-water produces a thicker thermal boundary layer with higher temperature as compared to the water–Cu nanofluid.

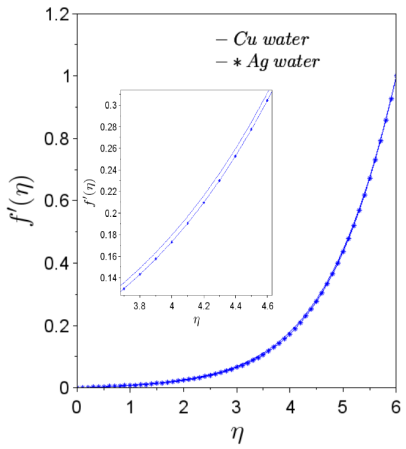

Fig. 12. Velocity profiles of Cu and Ag water nanofluids for Pr = 6.2, $M = 0.5$, Br = 0.1, $S_w = 0.2$, $\phi = 0.1$, $R = 1$ and $r_v = 1$

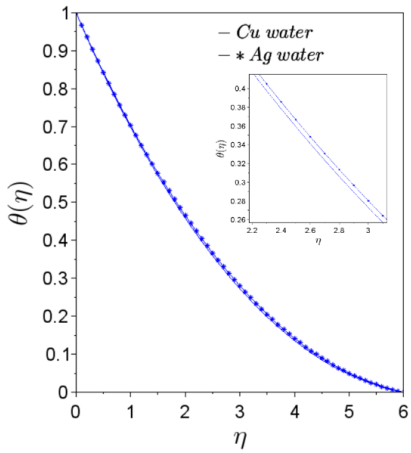

Fig. 13. Temperature profiles of Cu and Ag water nanofluids for Pr = 6.2, $M = 0.5$, Br = 0.1, $S_w = 0.2$, $\phi = 0.1$, $R = 1$ and $r_v = 1$

3.3. Effects of skin friction and Nusselt number

Fig. 14 shows that the skin friction coefficient increases with solid fraction ϕ. The skin friction coefficient tells us how much resistance one surface experienced when moving on another surface. Here, on increasing the volume of nanoparticles, the effective viscosity of the fluid as well as the interaction between the nanoparticles and the surface also increases. As a result, we observed an increment in the skin friction coefficient. Also, we observed that Cu-water nanofluid has a higher value of skin friction coefficient than Ag-water nanofluid.

The analysis in Fig. 15 shows that the Nusselt number increases with solid fraction ϕ. As we know, the Nusselt number is a measure of the efficiency of convective heat transfer to conductive heat transfer in a fluid. Here we observed that Cu-water nanofluid has a higher Nusselt number than Ag-water nanofluid. It means Cu-water nanofluid has higher thermal conductivity than Ag-water nanofluid.

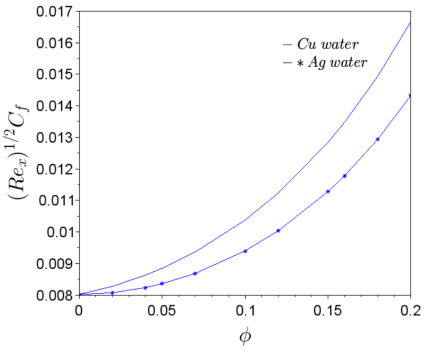

Fig. 14. Graph of skin friction of Cu and Ag water nanofluids

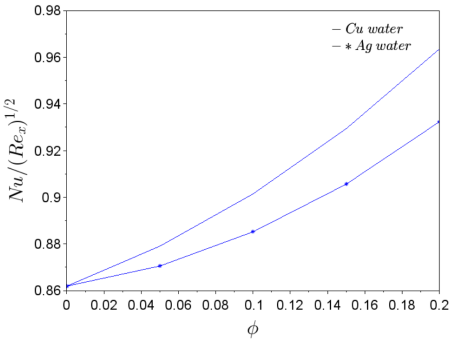

Fig. 15. Graph of Nusselt number of Cu and Ag water nanofluids

3.4. Comparison based on experimental study

Although the results presented in this study are derived purely from a mathematical 2D simulation, a comparative analysis has been conducted with the 2D numerical findings reported in Rehena Nasrin's thesis, "A 3D Numerical Study of Thermofluid Characteristics of a Flat Plate Solar Collector using Nanofluid" [38]. While Nasrin's work encompasses both 2D and 3D models, the comparison here is limited to her 2D results to maintain dimensional consistency. The trends observed in this study – specifically the increase in Nusselt number with rising Prandtl number, Reynolds number, and solid volume fraction – closely align with those documented in Nasrin's work.

For instance, Fig. 17 in this study shows the variation of Nusselt number with Reynolds number, which corresponds well with Figure 3.9(i) in Nasrin's thesis. Similarly, Fig. 19 illustrates the effect of Prandtl number on Nusselt number, matching the trend shown in Figure 3.11(i). The influence of solid volume fraction is depicted in Fig. 21, which aligns with Figure 3.13(i) in Nasrin's thesis. These consistent trends across both studies reinforce the reliability of the present 2D mathematical model and its ability to replicate thermofluid behavior observed in nanofluid-based solar collectors.

Furthermore, Nasrin's thesis [38] (Chapter 4, Section 4.5.4) highlights that within the 2D framework, the transverse cross-sectional model exhibits limitations in reliability compared to the longitudinal cross-sectional model. In our present study, we have adopted a longitudinal cross-sectional configuration for the flat plate, thereby aligning with the more robust modeling approach and reinforcing the validity of our simulation results.

In addition, Table 3 and Table 4 in this study present numerical data that further validate the observed trends. These tables clearly demonstrate the increasing values of the Nusselt number corresponding to rising Reynolds number, Prandtl number, and solid volume fraction.

Additionally, as shown in Table 2, Fig. 22, and Fig. 23, our results coincided precisely with those of Motsumi and Makinde [31] under the conditions of zero magnetic field ($M = 0$) and absence of a porous medium ($\lambda = 0$). This agreement serves as a benchmark for the accuracy and consistency of our numerical procedure.

Table 2. Computation of $\mathrm{Re}_x^{1/2} C_f$ showing comparison with [31] results for $\lambda = 0$, $S_w = 0$, $\mathrm{Br} = 0$, $R = \infty$, and $\mathrm{Pr} = 6.2$

ϕ	Cu-water			Ag-water		
	$M = 0$	$M = 1$	$M = 2$	$M = 0$	$M = 1$	$M = 2$
0	0.3321	0.0059	0.0006	0.3326	0.0059	0.0006
0.008	0.3459	0.0064	0.0007	0.3483	0.0064	0.0007
0.016	0.3597	0.0070	0.0008	0.3639	0.0070	0.0008
0.1	0.5076	0.0165	0.0022	0.5294	0.0171	0.0023
0.2	0.7066	0.0457	0.0077	0.7482	0.0494	0.0080

Fig. 16 shows Nasrin's thesis results, where the Nusselt number for nanofluid lies between about 1.8 and 2.1 for Reynolds numbers in the range of 400–500, while Fig. 17 presents the current study with values much higher, approximately 8.19–9.16. Similarly, Fig. 18 indicates Nasrin's Nusselt number variation with Prandtl number (≈ 1.9–2.3), whereas Fig. 19 shows our results in the range of 8.4–9.6. For solid volume fraction, Fig. 20 reports values of ≈ 1.8–2.2, while Fig. 21 demonstrates significantly higher values, around 8.7–9.1. These consistent differences arise because the moving flat plate in our model enhances shear and fluid mixing, maintains better nanoparticle dispersion, and disrupts the thermal boundary layer more effectively (as considered in the present work) than the confined riser pipe geometry (as considered in Nasrin's work). In addition, the increments in Nusselt number with different parameters can be explained as follows:

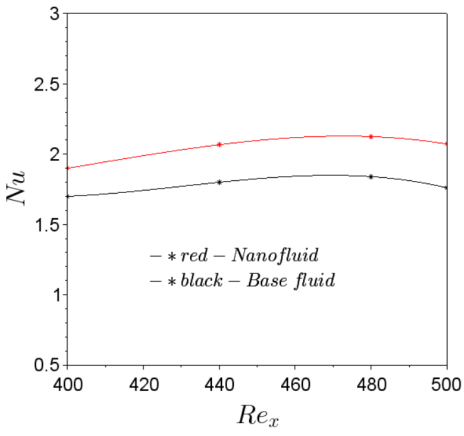

Fig. 16. Graph of Nu with Re from Nasrin's work

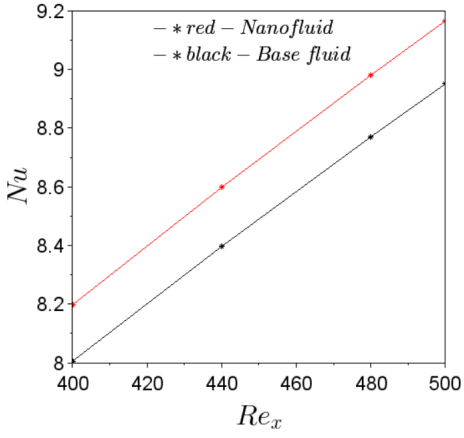

Fig. 17. Graph of Nu with Re_x

- **Reynolds number**: Higher Reynolds numbers correspond to stronger inertial forces and thinner hydrodynamic boundary layers. This intensifies convective transport and enhances heat transfer, leading to a rise in Nusselt number.
- **Prandtl number**: An increase in Prandtl number implies reduced thermal diffusivity relative to momentum diffusivity. This results in a thinner thermal boundary layer and stronger temperature gradients at the wall, thereby increasing the Nusselt number.
- **Solid volume fraction**: Adding more nanoparticles increases the effective thermal conductivity of the nanofluid. This improves energy transport within the fluid and strengthens convective heat transfer, which manifests as higher Nusselt numbers.

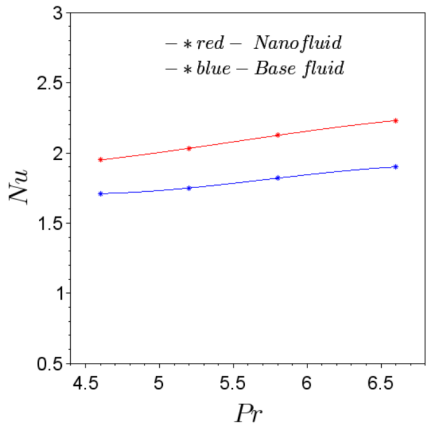

Fig. 18. Graph of Nu with Pr from Nasrin's work

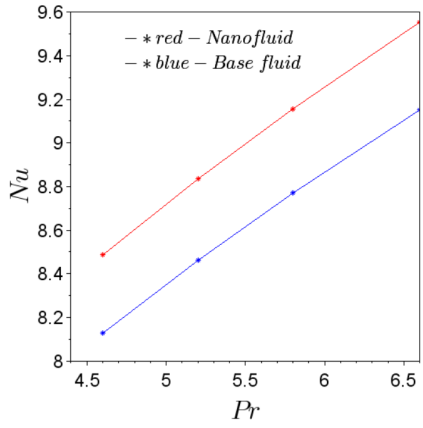

Fig. 19. Graph of Nu with Pr

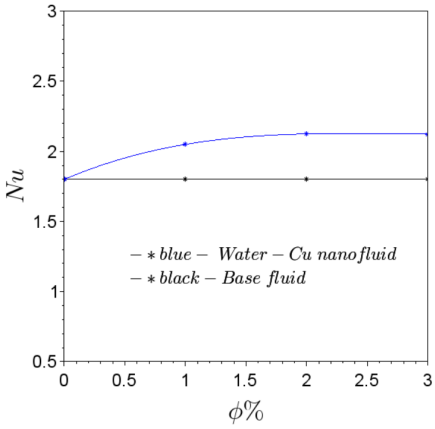

Fig. 20. Graph of Nu with ϕ% from Nasrin's work

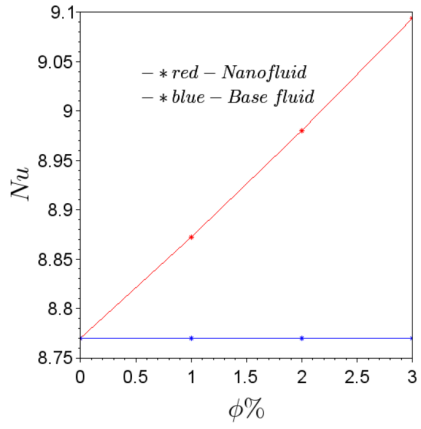

Fig. 21. Graph of Nu with ϕ%

It is important to note that while the absolute values of Nusselt number in our study are significantly higher than those reported by Nasrin, the overall trends with Reynolds number, Prandtl number, and solid volume fraction are similar in both works. This consistency in trends reinforces the physical validity of our model, even though the magnitude differences arise from variations in geometry, boundary conditions, and surface motion.

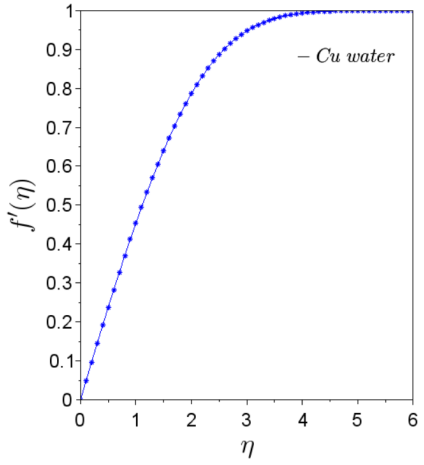

Fig. 22. Velocity profile of Cu-water nanofluid from Motsumi and Makinde [31]

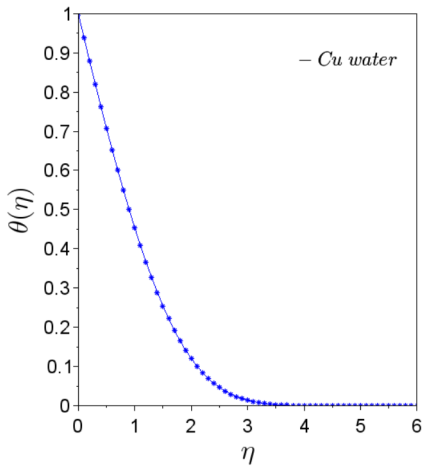

Fig. 23. Temperature profile of Cu-water nanofluid from Motsumi and Makinde [31]

Table 3. Computation of Nu for nanofluid showing results fo r $\lambda = 0$, $S_w = 0$, Br = 0, $M = 0$

ϕ%	Pr	Re_x	R	Nanofluid (Cu-water)
2%	4.6	480	215	8.48587
2%	5.2	480	215	8.83391
2%	5.8	480	215	9.15661
2%	6.6	480	215	9.55442
2%	5.8	400	215	8.19785
2%	5.8	440	215	8.59797
2%	5.8	480	215	8.98029
2%	5.8	500	215	9.16547
0%	5.8	480	215	8.76998
1%	5.8	480	215	8.87223
2%	5.8	480	215	8.98029
3%	5.8	480	215	9.09401

Table 4. Computation of Nu for clear fluid showing results for $\lambda = 0$, $S_w = 0$, Br $= 0$, $M = 0$

ϕ%	Pr	Re_x	R	Clear fluid
0%	4.6	480	215	8.12655
0%	5.2	480	215	8.46047
0%	5.8	480	215	8.76998
0%	6.6	480	215	9.1515
0%	5.8	400	215	8.00586
0%	5.8	440	215	8.39662
0%	5.8	480	215	8.76998
0%	5.8	500	215	8.95083

4. Conclusions

This study investigates the flow and heat transfer characteristics of copper (Cu) and silver (Ag) nanofluids over a permeable, moving flat plate subjected to a magnetic field and embedded in a porous medium. The model incorporates the effects of suction/injection, nanoparticle volume fraction, thermal radiation, and viscous dissipation. Governing equations are transformed using similarity transformations and solved numerically via the fourth-order Runge–Kutta method with a shooting technique. Results show that the magnetic field and porosity parameters collectively enhance the velocity until it stabilizes.

Ag–water nanofluid exhibits higher temperature distributions, while Cu–water demonstrates greater skin friction and Nusselt numbers, indicating superior heat transfer. Velocity profiles decrease with increasing magnetic field strength, porosity, volume fraction, and suction/injection rate. The thermal boundary layer thickens with higher values of magnetic parameter, porosity, and volume fraction, but becomes thinner with stronger suction or injection. Temperature rises with increased Brinkman number and decreases with stronger thermal radiation.

Graphical analysis reveals an approximate 20% reduction in velocity for each increment in suction/injection parameter (S_w), a 12.90% drop from $\phi = 0$ to $\phi = 0.1$, and a 1.85% drop from $\phi = 0.1$ to $\phi = 0.2$. Velocity decreases by 44.16% between $\lambda = 0$ and $\lambda = 1$, and by 30.23% between $\lambda = 1$ and $\lambda = 2$, with about a 26% drop for each unit increase in magnetic parameter M. For temperature, a reduction of approximately 31.25% is observed between $S_w = 0$ and $S_w = 0.5$, and 45.45% between $S_w = 0.5$ and $S_w = 1$; it also reduces by 25.93% from $R = 0.5$ to $R = 1$ and 20% from $R = 1$ to $R = 2$. Temperature increases by 18.84% from $\phi = 0$ to $\phi = 0.1$, and 24.39% from $\phi = 0.1$ to $\phi = 0.2$; it also rises by 15.38% from $\lambda = 0$ to $\lambda = 1$, and 10.89% from $\lambda = 1$ to $\lambda = 2$; it also increases by 10% from $M = 0$ to $M = 1$, and 4.55% from $M = 1$ to $M = 2$, 14.13% from Br $= 1$ to Br $= 2$, and 12.38% from Br $= 2$ to Br $= 3$. The

findings highlight the improved heat transfer capability of Cu–water nanofluid and provide valuable insights for designing thermal systems that function in porous and magnetohydrodynamic environments.

References

[1] S.U.S. Choi and Jeffrey Eastman. Enhancing thermal conductivity of fluids with nanoparticles. *Proceedings of the ASME International Mechanical Engineering Congress and Exposition*, 66:99–105, 1995.

[2] J. Buongiorno. Convective transport in nanofluids. *ASME Journal of Heat Transfer*, 128:240–250, 2006. doi: 10.1115/1.2150834.

[3] M. Sheikholeslami, M.M. Rashidi, and D.D. Ganji. Effect of nonuniform magnetic field on forced convection heat transfer of Fe3O4–water nanofluid. *Computational Methods in Applied Mechanics and Engineering*, 294:299–312, 2015. doi: 10.1016/j.cma.2015.06.010.

[4] M. Hatami, M. Khazayinejad, and D. Jing. Forced convection of Al2O3–water nanofluid flow over a porous plate under the variable magnetic field effect. *International Journal of Heat and Mass Transfer*, 102:622–630, 2016. doi: 10.1016/j.aej.2017.03.018.

[5] Nurul Amira Zainal, Roslinda Nazar, Kohilavani Naganthran, and Ioan Pop. MHD mixed convection stagnation point flow of a hybrid nanofluid past a vertical flat plate with convective boundary condition. *Chinese Journal of Physics*, 66:630–644, 2020. doi: 10.1016/j.cjph.2020.03.022.

[6] Najiyah Safwa Khashi'ie, Norihan Md Arifin, and Ioan Pop. Magnetohydrodynamics (MHD) boundary layer flow of hybrid nanofluid over a moving plate with joule heating. *Alexandria Engineering Journal*, 61(3):1938–1945, 2022. doi: 10.1016/j.aej.2021.07.032.

[7] Basant K. Jha and Gabriel Samaila. Thermal radiation effect on boundary layer over a flat plate having convective surface boundary condition. *SN Applied Sciences*, 2(381):1–8, 2020. doi: 10.1007/s42452-020-2167-8.

[8] R. Cortell. Effects of viscous dissipation and radiation on the thermal boundary layer over a nonlinearly stretching sheet. *Physics Letters A*, 372(5):631–636, 2008. doi: 10.1016/j.physleta.2007.08.005.

[9] A. Raptis, C. Perdikis, and H. S. Takhar. Effect of thermal radiation on MHD flow. *Applied Mathematics and Computation*, 153(3):645–649, 2004. doi: 10.1016/S0096-3003(03)00657-X.

[10] S. Arulmozhi, K. Sukkiramathi, S. S. Santra, and S. Nandi. Impact of thermal radiation on water-based hybrid nanofluid (Cu–Al_2O_3–H_2O) flow over a forward/backward moving vertical porous plate. *Arabian Journal for Science and Engineering*, 50:477–487, 2025. doi: 10.1007/s13369-024-09108-0.

[11] Ammar Jafaripournimchahi, Amirali Shateri, Bahram Jalili, Payam Jalili, and Davood Domiri Ganji. The effects of magnetic field and thermal radiation on the mixed convection of Al_2O_3-Cu/water hybrid nanofluid over a permeable vertical flat plate. *Modern Physics Letters B*, 38(25):2450242, 2024. doi: 10.1142/S0217984924502427.

[12] Funmilayo H. Oyelami and Bidemi O. Falodun. Heat and mass transfer of hydrodynamic boundary layer flow along a flat plate with the influence of variable temperature and viscous dissipation. *International Journal of Heat and Technology*, 39(2):441–450, April 2021. doi: 10.18280/ijht.390213.

[13] H. C. Brinkman. Heat transfer in capillary flow I. *Applied Science Research*, 2:120–124, 1951. doi: 10.1007/BF00411976.

[14] Najiyah Safwa Khashi'ie, Iskandar Waini, Anuar Ishak, and Ioan Pop. Blasius flow over a permeable moving flat plate containing Cu-Al_2O_3 hybrid nanoparticles with viscous dissipation and radiative heat transfer. *Mathematics*, 10(8):1281, 2022. doi: 10.3390/math10081281.

[15] Himanshu Upreti, Alok Kumar Pandey, and Manoj Kumar. MHD flow of Ag-water nanofluid over a flat porous plate with viscous-ohmic dissipation, suction/injection and heat generation/absorption. *Alexandria Engineering Journal*, 57(3):1839–1847, 2018. doi: 10.1016/j.aej.2017.03.018.

[16] D. Gopal, S. Saleem, S. Jagadha, Farooq Ahmad, A. Othman Almatroud, and N. Kishan. Numerical analysis of higher order chemical reaction on electrically MHD nanofluid under influence of viscous dissipation. *Alexandria Engineering Journal*, 60(1):1861–1871, 2021. doi: 10.1016/j.aej.2020.11.034.

[17] Yap Bing Kho, Rahimah Jusoh, Mohd Zuki Salleh, Mohd Hisyam Ariff, and Nooraini Zainuddin. Magnetohydrodynamics flow of Ag-TiO_2 hybrid nanofluid over a permeable wedge with thermal radiation and viscous dissipation. *Journal of Magnetism and Magnetic Materials*, 565:170284, 2023. doi: 10.1016/j.jmmm.2022.170284.

[18] D. Iranian, K. Sudarmozhi, Ilyas Khan, and Abdullah Mohamed. Significance of heat generation and impact of suction/injection on Maxwell fluid over a horizontal plate by the influence of radiation. *International Journal of Thermofluids*, 20:100396, 2023. doi: 10.1016/j.ijft.2023.100396.

[19] Moh Yaseen, Rashmi Garia, Sawan Kumar Rawat, and Manoj Kumar. Hybrid nanofluid flow over a vertical flat plate with Marangoni convection in the presence of quadratic thermal radiation and exponential heat source. *International Journal of Ambient Energy*, 44(1):527–541, 2023. doi: 10.1080/01430750.2022.2132287.

[20] Muhammad Shuaib, Abbas Ali, Muhammad Altaf Khan, and Aatif Ali. Numerical investigation of an unsteady nanofluid flow with magnetic and suction effects to the moving upper plate. *Advances in Mechanical Engineering*, 12(2):168781402090358, 2020. doi: 10.1177/1687814020903588.

[21] V. K. Verma and A. F. Ansari. Darcy-Brinkman flow in an anisotropic rotating porous channel under the influence of magnetic field. *Journal of Porous Media*, 27(6):31–43, 2024.

[22] V. K. Verma and A. F. Ansari. Effect of magnetic field on Darcy-Brinkman flow through rotating porous channel system. *Special Topics & Reviews in Porous Media*, 16(3):99–110, 2025. doi: 10.1615/SpecialTopicsRevPorousMedia.2024052434.

[23] V. K. Verma and A. F. Ansari. Effect of magnetic field and slip conditions on flow in a rotating porous channel with viscous dissipation. *Heat Transfer*, 54(2):1562–1573, 2025. doi: https://doi.org/10.1002/htj.23241.

[24] A. F. Ansari. Role of inclined magnetic field on couette slip flow and heat transfer with viscous dissipation in a rotating porous channel: Application in pumping systems. *Phys Fluids*, 37(8):085108, 2025. doi: 10.1063/5.0288181.

[25] Abdul Faiz Ansari and Vineet Kumar Verma. MHD casson fluid past an exponentially stretching plane in a porous medium. *Journal of Porous Media*, 2025. Advance Online Publication.

[26] V. K. Verma and A. F. Ansari. Couette flow through an anisotropic porous rotating channel: Brinkman approach. *Z Angew Math Mech*, 105(1):e202400353, 2024. doi: 10.1002/zamm.202400353.

[27] S. Ahmad and I. Pop. Mixed convection boundary layer flow from a vertical flat plate embedded in a porous medium filled with nanofluids. *Int Commun Heat Mass Transfer*, 37(8):987–991, October 2010. doi: 10.1016/j.icheatmasstransfer.2010.06.004.

[28] M. K. Awasthi, A. K. Shukla, A. K. Singh, and P. Shukla. Interfacial instability analysis of viscous-viscoelastic fluid interface in an annular porous medium. *Journal of Porous Media*, 26(11):1–13, 2023. doi: 10.1615/JPorMedia.2023044861.

[29] V. K. Verma and A. F. Ansari. Darcy-Brinkman flow of a micropolar fluid through an anisotropic porous channel. *Journal of Computational and Theoretical Transport*, 53(7):575–594, 2024. doi: 10.1080/23324309.2024.2413187.

[30] V. K. Verma and A. F. Ansari. Couette flow of micropolar fluid in a channel filled with anisotropic porous medium. *Archive of Mechanical Engineering*, 71(4):581–596, 2024. doi: 10.24425/ame.2024.151336.

[31] T. G. Motsumi and O. D. Makinde. Effects of thermal radiation and viscous dissipation on boundary layer flow of nanofluids over a permeable moving flat plate. *Physica Scripta*, 86:045003, 2012. doi: 10.1088/0031-8949/86/04/045003.

[32] P. Keblinski, S. R. Phillpot, S. U. S. Choi, and J. A. Eastman. Mechanism of heat flow in suspensions of nano-sized particles (nanofluids). *International Journal of Heat and Mass Transfer*, 45(4):855–863, 2002. doi: 10.1016/S0017-9310(01)00175-2.

[33] X. Wang, X. Xu, and S. U. S. Choi. Thermal conductivity of nanoparticle fluid mixture. *Journal of Thermophysics and Heat Transfer*, 13(4):474–480, 1999. doi: 10.2514/2.6486.

[34] J. A. Eastman, S. U. S. Choi, S. Li, W. Yu, and L. J. Thompson. Anomalously increased effective thermal conductivity of ethylene glycol-based nanofluids containing copper nanoparticles. *Applied Physics Letters*, 78(6):718–720, 2001. doi: 10.1063/1.1341218.

[35] S. Ahmad, A. M. Rohni, and I. Pop. Blasius and Sakiadis problems in nanofluids. *Acta Mechanica*, 218(3):195–204, 2011. doi: 10.1007/s00707-010-0414-6.

[36] R. K. Tiwari and M. K. Das. Heat transfer augmentation in a two-sided lid-driven differentially heated square cavity utilizing nanofluids. *International Journal of Heat and Mass Transfer*, 50(9–10):2002–2018, 2007. doi: 10.1016/j.ijheatmasstransfer.2006.09.034.

[37] O. D. Makinde. Free-convection flow with thermal radiation and mass transfer past a moving vertical porous plate. *International Communications in Heat and Mass Transfer*, 32(10):1411–1419, 2005. doi: 10.1016/j.icheatmasstransfer.2005.07.005.

[38] Rehena Nasrin. *A 3D Numerical Study of Thermofluid Characteristics of a Flat Plate Solar Collector Using Nanofluid*. Department of Mathematics, Bangladesh University of Engineering and Technology, Dhaka-1000, Bangladesh, August 2015.